Broadband sub-wavelength profile high-gain antennas based on multi-layer metasurfaces

Konstantinidis, Konstantinos; Feresidis, Alexandros P.; Hall, Peter S.

DOI:
10.1109/TAP.2014.2365825

License:
Other (please specify with Rights Statement)

Document Version
Peer reviewed version

Citation for published version (Harvard):
Konstantinidis, K, Feresidis, AP & Hall, PS 2015, 'Broadband sub-wavelength profile high-gain antennas based on multi-layer metasurfaces', *IEEE Transactions on Antennas and Propagation*, vol. 63, no. 1, 6940214, pp. 423-427. https://doi.org/10.1109/TAP.2014.2365825

Broadband Sub–Wavelength Profile High-Gain Antennas Based on Multi-layer Metasurfaces

Konstantinos Konstantinidis, Alexandros P. Feresidis, *Senior Member, IEEE* and Peter S. Hall, *Fellow, IEEE*

***Abstract*— A method for designing sub-wavelength-profile and broadband high-gain planar antennas is presented. A novel multi-layer periodic array design is proposed for sub-wavelength Fabry-Perot cavity type antennas with enhanced bandwidth performance. Three double-sided periodic arrays are designed and optimised, each double-sided array consisting of a capacitive Artificial Impedance Surface (AIS) and an inductive Partially Reflective Surface (PRS) printed on either side of a dielectric substrate. They are placed at about sixth of a wavelength from a ground plane and from each other. Thus, three air cavities are created with a total profile of λ/2. The proposed antenna has been simulated using CST Microwave Studio™ and measured achieving 16.9dBi directivity with 10.7% 3dB bandwidth. The gain-bandwidth product of the measured prototype outperforms any previous Fabry-Perot antenna design with this profile.**

***Index Terms*— Fabry-Perot cavity; Artificial magnetic conductor; Partially reflective surfaces; Leaky-wave antennas.**

I. Introduction

Metamaterial based structures have been extensively employed in recent years to achieve antenna directivity enhancement [1-3]. A typical implementation of planar highly directive antennas that has attracted significant interest in the past is based on periodic superstrates to create Fabry-perot cavity (FPC) type leaky wave antennas [4, 5]. These designs provide high efficiency and eliminate the need for a complex feeding network. The superstrate, typically formed by a doubly periodic array of elements, is placed at approximately half wavelength distance over a metallic ground plane and a low-directivity primary source (e.g. dipole). The periodic array acts as a Partially Reflective Surface (PRS), which suggests that a leaky-wave approach can be adopted to interpret the operation of the formed antenna [6-8]. Moreover, a ray optics theory has been successfully employed to describe the operation of this type of antennas and estimate the

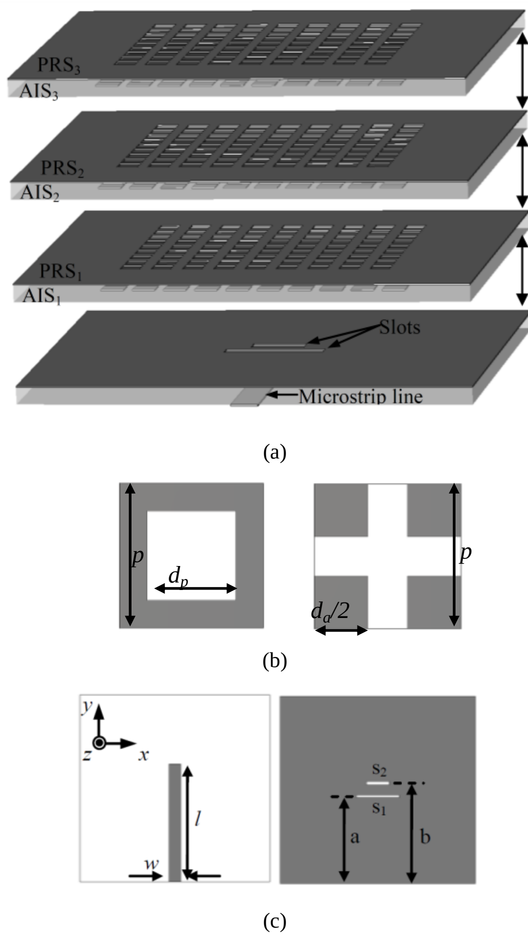

Fig. 1. (a) Schematic diagram of the proposed antenna (dimensions are not to scale), (b) top (PRS array) and bottom (AIS array) view of the unit cell, (c) back and front view of ground plane with the microstrip line and slots.

directivity performance [9, 10]. According to this theory, maximum directivity is achieved when constructive interference occurs between the direct rays emerging from the primary source and the reflected rays which undergo multiple reflections between the ground plane and the PRS [9, 10].

Due to the resonance related operation of FPC antennas, they suffer from narrow bandwidth. Recently, a technique for bandwidth improvement was introduced [11] using the coupling between two surfaces to obtain a positive phase gradient that satisfies the resonance condition of the antenna cavity for a certain frequency range. This technique was further investigated in more recent works employing different

Manuscript received July 10, 2014. This work was supported by the UK EPSRC under Grant EP/J500367/1. A. P. Feresidis wishes to acknowledge the support by the Royal Academy of Engineering and The Leverhulme Trust under a senior research fellowship.

K. Konstantinidis, A. P. Feresidis and P. S. Hall are with the School of Electronic, Electrical and Computer Engineering, University of Birmingham, Edgbaston, Birmingham B15 2TT, U.K.

configurations [12-16]. However, this technique implies an increase to the total antenna profile, since the coupled surfaces have a large separation of half wavelength between them and also from the ground plane, resulting to a total profile of over a wavelength.

The profile reduction of FPC type antennas has also been studied extensively by replacing the ground plane with an Artificial Magnetic Conductor (AMC). AMCs are formed by a periodic arrangement of metallic patches on a grounded dielectric substrate and were first introduced by Sievenpiper *et al.*[17]. Their key property is that they reflect electromagnetic waves with zero phase shift at a specific frequency. This property has been exploited to obtain λ/4 profile highly directive antennas [18-22]. A further profile reduction has been proposed demonstrating operation of sub-wavelength cavity modes (~λ/16) [23] and an ultrathin directive antenna (~λ/60) [24], both employing an AMC ground plane and a combination of an AMC and a PRS superstrate. However, all the above designs were characterized by narrow bandwidth. Recently, a first report of a method to achieve bandwidth enhancement of sub-wavelength profile FPC was presented in [25].

In this paper, we present a novel multilayer sub-wavelength profile FPC antenna with a significantly increased bandwidth performance (Fig. 1a). Three double-sided arrays are employed each one consisting of an Artificial Impedance Surface (AIS) and a PRS surface with sub-wavelength unit cell dimensions printed on either sides of a dielectric substrate. They are placed at a distance of about λ/6 from a ground plane and from each other. Thus, three air cavities are created with a total profile of ~λ/2. The elements on both AIS and PRS surfaces are sub-wavelength and non-resonant in the frequency range of interest (Fig. 1b). Two optimised microstrip-fed slots are used as a low directivity source to excite the sub-wavelength cavities (Fig. 1c). A periodic analysis is initially carried out to extract the reflection characteristics of the surfaces and estimate the antenna performance. Three finite size antennas are presented using a single-layer, a double-layer and a three-layer AIS-PRS respectively.

This paper is organized as follows. The design of a single-layer AIS-PRS for a λ/6 profile antenna is described in Section II (A), including periodic analysis. Then, a double-layer structure is presented in Section II (B) employing two pairs of AIS-PRS surfaces. Subsequently, a three-layer structure designed formed by three composite AIS-PRS surfaces at a distance of λ/6 from each other, is analyzed in Section II (C). In Section III the design and comparison of three finite size antennas based on the periodic analysis in the previous sections is carried out as well as a comparison between the proposed three-layer AIS-PRS antenna and a conventional single-layer Fabry-Perot antenna of λ/2 profile in terms of directivity and bandwidth. Fabrication and measurements of the proposed three-layer antenna are presented in Section IV and finally conclusions are given in Section V.

II. Unit Cell Design of AIS-PRS

A. *Single-layer AIS-PRS*

Initially a single layer AIS-PRS structure is designed. The AIS and PRS arrays are printed on both sides of a 1.55mm thick dielectric substrate with ε_r=2.2. The AIS array is formed by square metallic patches with a periodicity p=5.5mm, while the PRS array is formed by square apertures with the same periodicity, shifted with respect to the AIS array by $p/2$ in x and y-axis. The unit cell dimensions are shown in Fig. 1(b) for the bottom (AIS) side and for the top (PRS) side, with d_p=3mm and d_a=4.4mm. In order to create a λ/6 cavity, the reflection phase of the structure ϕ_R has to satisfy (1) for h=λ/6 (π is the phase introduced by the total reflection at the ground), i.e. to be -60^o at the desired operating frequency, with high reflection magnitude values to achieve a high directivity antenna. The phase is controlled predominantly by the dimensions of the AIS while the magnitude by the aperture size of the PRS. Therefore the dimensions of the unit cell have been carefully selected to obtain the required reflection phase at 14GHz. Periodic boundary conditions are applied in the simulation software, assuming an infinite structure to extract the reflection coefficients. The simulated reflection characteristics are presented in Fig. 2. It can be observed that high values of magnitude are obtained due to the highly reflective PRS and a reflection phase of -60^o is obtained at 14GHz.

$$\phi_R - \pi - \frac{2\pi}{\lambda}2h = \pm 2N\pi, \quad N=0,1,2... \quad (1)$$

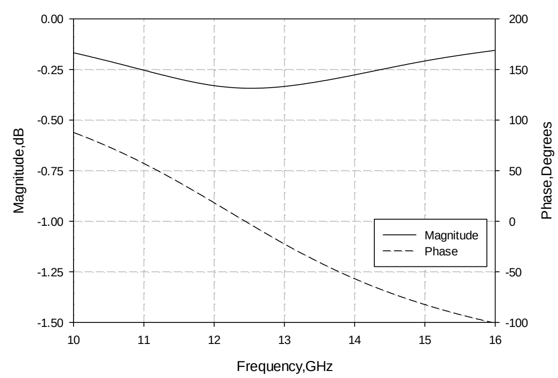

Fig. 2. Reflection magnitude and phase of single layer AIS-PRS.

B. *Double-layer AIS-PRS*

Next, the concept of the sub-wavelength profile antenna is extended for multilayer structures. In this section, a double layer structure is designed employing two composite surfaces of AIS-PRS. Initially the first layer is designed following the procedure that was followed for the design of the single AIS-PRS layer. The dimensions are chosen such that high reflection magnitude values and a reflection phase of -60^o are obtained. Next, a second layer is added at λ/6 distance from the first one. The resonance condition (2) for the second cavity is derived from (1) after replacing the reflection phase π from the ground plane with ψ_{R1} which is the reflection phase at the first layer from the PRS side. In this case, the reflection phase at the second layer from the AIS side is ϕ_{R2} (Fig. 3). Since ψ_{R1} is replacing the full reflection from the ground plane, the PRS of the first layer should be designed to achieve a phase of around π (180°). Substituting h_2 with λ/6 in (3), which arises rearranging equation (2), the value of ϕ_{R2} can be calculated. For N=1 and ψ_{R1}=172°, it can be extracted that ϕ_{R2} should be -68° at the operational frequency for the equation to be satisfied.

$$\phi_{R2} - \psi_{R1} - \frac{2\pi}{\lambda} 2h_2 = \pm 2N\pi, \quad N=0,1,2... \quad (2)$$

$$h_2 = \left(\frac{\phi_{R2}}{\psi_{R1}} - \frac{\pi}{\psi_{R1}}\right)\frac{\lambda}{4} + N\frac{\lambda}{2}, \qquad N=0,1,2... \quad (3)$$

Periodic boundary conditions are then applied to the unit cell of the multilayer structure and the reflection coefficients are extracted. The dimensions are shown in Fig. 3 with d_{p1}=3mm, d_{p2}=3.6mm, d_{a1}=d_{a2}=4.4mm and h_2=3.6mm. Furthermore the thickness of the first cavity is h_1=4mm. These dimensions are chosen after investigation, in order to obtain the desired values for the reflection phases ϕ_{R1}, ϕ_{R2} and ψ_{R1}. The phase and magnitude for reflection at the PRS_1 (first layer) are presented in Fig. 4. High magnitude values are obtained, while the reflection phase ψ_{R1} is stable at 172° around the resonant frequency. For the second layer, the complex reflection coefficient at the side of AIS_2 is shown in Fig. 5. It can be observed that the reflection phase ϕ_{R2} is -70° around 14GHz. Inserting the values of ψ_{R1} and ϕ_{R2} for f=14GHz at (3) the cavity distance is h_2=3.53mm which is in good agreement with the actual value that has been used. Finally, the complex reflection coefficient for incidence at AIS_1, including the complete double layer unit cell in the simulation, is presented in Fig. 6. It should be noted at this point that the selection of the aperture size of the PRSs has been such that a phase increase would be achieved in the frequency range of operation. This derives from (1), which shows that for a maximum directivity within a certain frequency range, a linearly-increasing-with-frequency phase response is required. Indeed, from Fig. 6 it can be observed that a phase increase occurs for ϕ_{R1}, between 13.6GHz and 13.8GHz. The theoretical phase derived from (1) for h_1=4mm is also included in the graph. It is expected that at the frequencies where the two phase responses intersect, the directivity will be maximum. Moreover, the reflection phase ϕ_{R1} is -50° at 13.7GHz, resulting in a cavity thickness of h_1=3.95mm from the ray optics analysis, which again is close to the actual value that has been used for the design.

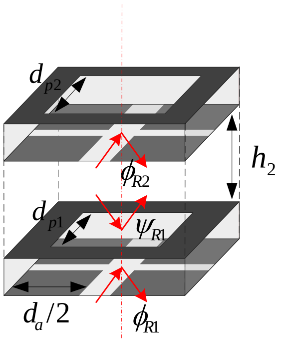

Fig. 3. Unit cell of the double layer structure.

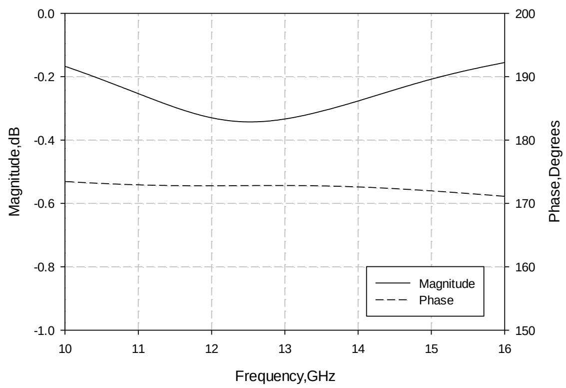

Fig. 4. Reflection magnitude and phase at PRS_1.

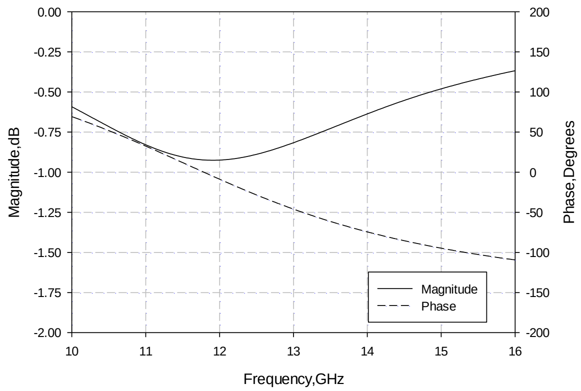

Fig. 5. Reflection magnitude and phase at AIS_2

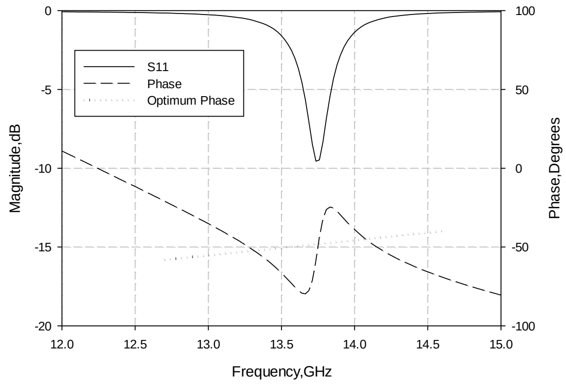

Fig. 6. Reflection magnitude and phase of the double layer AIS-PRS.

C. Three-layer AIS-PRS

In this subsection a three-layer AIS-PRS structure is presented. It must be emphasized that all three AIS-PRS layers in this design are different from the double-layer structure presented in the previous section II (B). Based on the conclusion extracted from the analysis in the previous subsection, the concept is further extended here to the design of three composite AIS-PRS layers of sub-wavelength profile. The unit cell of the structure is shown in Fig. 7. The first two layers are designed to satisfy (2) and (3) as described in the previous sections. For the third layer the dimensions are chosen such that the reflection phase ϕ_{R3} will result in a cavity of h_3= λ/6 at the central frequency. The new optimised dimensions are d_{p1}=3.5mm, d_{p2}=3.1mm, d_{p3}=4.3mm, $d_{a1}=d_{a2}=d_{a3}$=4.4mm, h_2=3.9mm and h_3=2.64mm (Fig. 7). Also, the first cavity thickness h_1 is set at 3.65mm (Fig. 1a).

Periodic boundary conditions are applied to the unit cell of the structure and the reflection characteristics are calculated. For incidence at PRS_1, the magnitude and phase of the reflection coefficients are presented in Fig. 8. For incidence at the AIS_2 (second layer) the reflection magnitude and phase are presented in Fig. 9. It can be seen from Fig. 8 and Fig. 9 that the reflection phases ψ_{R1} and ϕ_{R2} at 13.7GHz, are 171^o and -53^o respectively. These values correspond to a cavity thickness h_2=4.1mm which is close to the optimised one. In Fig. 10 and Fig. 11, the reflection coefficients for incidence at PRS_2 and AIS_3 are depicted respectively. In this case, the reflection phases ψ_{R2} at 13.7GHz is 188^o, while ϕ_{R3}=-90^o at the same frequency. Substituting this values in the resonance condition for the third cavity, gives h_3=2.5mm. Finally, the reflection coefficients of the complete structure, for incidence at the first layer (AIS_1) are shown in Fig. 12. It can be observed that a double reflection phase increase with frequency is obtained for ϕ_{R1} from 13.1GHz to 14.2GHz. The theoretical ideal phase for h_1=3.65mm is again included in the graph. The obtained phase follows closely the ideal phase indicating that a more broadband antenna performance for this optimised three layer structure is expected. Moreover, the reflection phase ϕ_{R1} is -65^o at 13.7GHz, giving a cavity thickness of h_1=3.5mm which determines the distance from the ground plane (Fig. 1a).

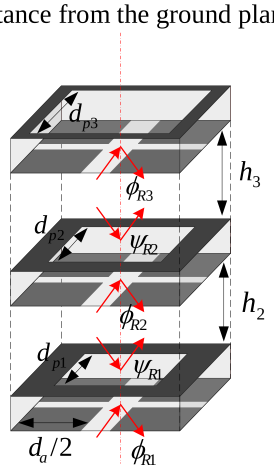

Fig. 7. Unit cell of the three layer structure.

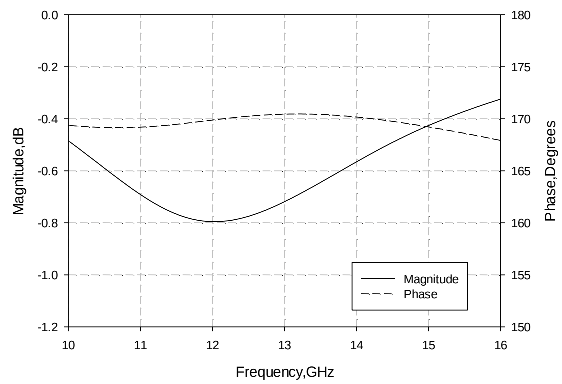

Fig. 8. Reflection magnitude and phase at PRS_1.

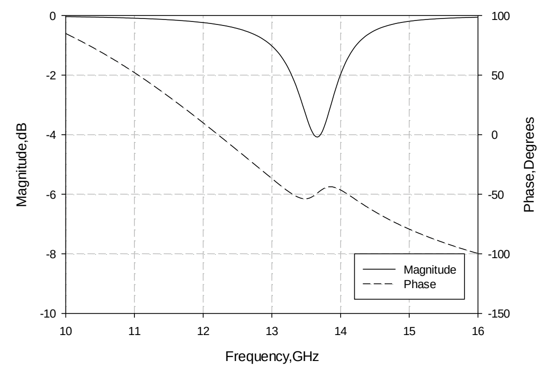

Fig. 9. Reflection magnitude and phase at AIS_2.

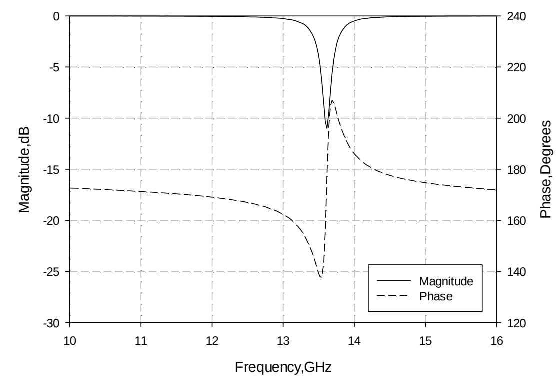

Fig. 10. Reflection magnitude and phase at PRS_2.

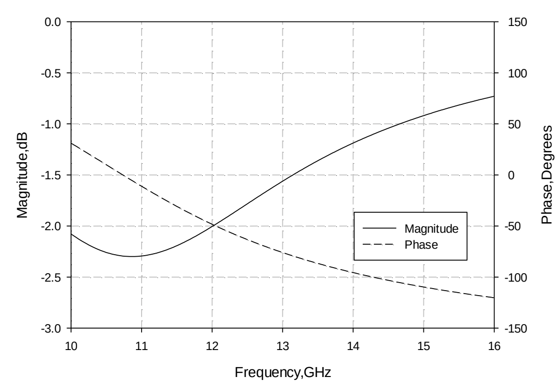

Fig. 11. Reflection magnitude and phase at AIS_3.

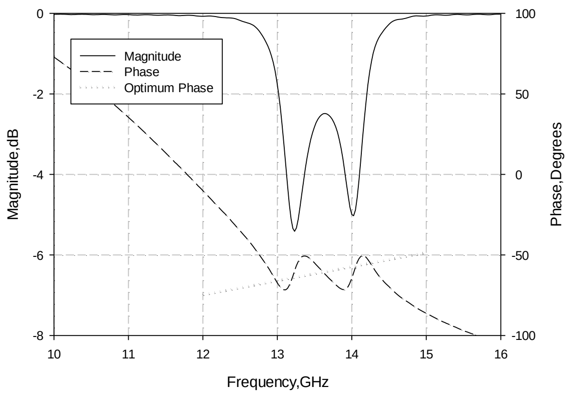

Fig. 12. Reflection magnitude and phase of the three layer AIS-PRS.

III. Finite Size Antennas

A. AIS-PRS antenna designs

Based on the conclusions from the previous section, three sub-wavelength finite size antennas are designed: a single-layer AIS-PRS, a double-layer AIS-PRS and a three-layer AIS-PRS antenna. Initially the single-layer antenna is introduced. It consists of an AIS-PRS array placed at distance *h* from a ground plane with 80 mm x 80 mm overall dimensions. The dimensions of the elements are as described in Section II (A). The cavity distance is set at *h*=3.8mm to obtain an optimised performance which is slightly more than λ/6 at 14GHz (3.6mm). This small discrepancy between the ray optics analysis and the finite size antenna is due to the fact that the former assumes an infinite structure. A novel feeding technique has been used to excite the antenna comprising a dual slot at the ground plane, fed by a microstrip line (Fig. 1c). The feeding structure is dual resonant, resulting in a wideband matching. The dimensions of s_1 are 17.5mm x 1mm and of s_2 are 9.4mm x 1.5mm. Moreover, from Fig. 1(c), a=37.2mm and b=42.8mm while the length and width of the microstrip line are *l*=50.5mm and *w*=4.8mm respectively. The ground plane and the microstrip line are printed on the same substrate (thickness 1.55mm and ε_r=2.2) as the composite AIS-PRS surfaces. The simulated directivity versus frequency is presented in Fig. 13. A maximum of 17dBi is achieved at 14.25GHz.

Subsequently, a finite size antenna was implemented employing the double-layer AIS-PRS of Section II (B). The structure is similar with the one shown in Fig. 1(a) but without the top AIS-PRS layer. The overall lateral dimensions of the structure are as in the single AIS-PRS layer antenna, while the cavity distances and the dimensions of the periodic elements are those mentioned in Section II (B). The profile of the antenna is h_1+h_2 which is about λ/3. The two microstrip line fed slots have been used again as excitation. The simulated directivity of the antenna versus frequency is also presented in Fig. 13. A maximum of 17.2dBi is achieved at 14.2GHz. It is interesting to note that two peaks appear in the directivity response, corresponding to the resonant modes of the two coupled cavities. It can be observed that an improved bandwidth performance is achieved with the proposed double AIS-PRS layer configuration compared to the single AIS-PRS layer antenna. This performance demonstrates that a broadband sub-wavelength profile highly-directive antenna is feasible through the introduction of an extra optimised composite AIS-PRS layers. It should be emphasized that even with a profile of less than λ/2, high directivity and broad bandwidth is achieved.

Finally, based on the periodic analysis of the three AIS-PRS layer structure, a three-layer finite size antenna has been implemented as shown in Fig. 1(a). The antenna has the same overall lateral size like the previous two cases. The dimensions of the elements and the cavity distances are those mentioned in Section II (C). The total profile of the antenna in this case is $h_1+h_2+ h_3$ which is approximately λ/2. The double-slot feeding structure is used again, to ensure a matching covering the antenna's operation frequency range (see Section IV). The simulated directivity response of the antenna is presented again in Fig. 13. A maximum of 16.9dBi is achieved at 13.8GHz with a 3dB radiation bandwidth of 10.7%. A fluctuation of less than 2dB is observed over the operational bandwidth. The antenna dimensions could be further optimised to achieve a more flat directivity response. Comparing the three aforementioned antenna designs presented in the figure, it is evident that the three AIS-PRS layer antenna achieves a more broadband performance. It can also be observed that three peaks occur in the directivity curve in the latter case, corresponding to the three resonant modes. A more detailed comparison between the three designs in terms of maximum directivity and 3dB bandwidth is presented in Table I.

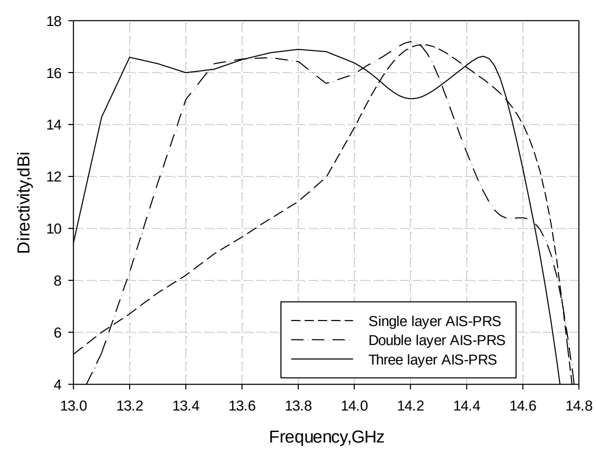

Fig. 13. Directivity vs frequency for the three proposed AIS-PRS antenna configurations.

TABLE I. Comparison of the Three AIS-PRS Antenna Configurations

Antenna Design	***Directivity max (dBi)***	***Bandwidth 3dB***
Single-Layer AIS-PRS	17	4.1%
Double-Layer AIS-PRS	17.2	7%
Three-Layer AIS-PRS	16.9	10.7%

B. Comparison with a Conventional λ/2 Profile Fabry-Perot PRS Antenna

In this subsection, a comparison of the proposed three AIS-PRS layer antenna with a conventional λ/2 profile Fabry-Perot antenna is carried out. The antenna under study consists of one layer aperture PRS placed at half wavelength distance in front of a ground plane. It is fed using the same feeding technique comprising the microstrip line fed slots. The investigated structure has been designed to operate in the same frequency band and achieve the same maximum directivity as the proposed antenna so that a fair comparison can be performed. In Fig. 14, the directivity versus frequency for the two evaluated designs is shown. The conventional Fabry-Perot antenna achieves a maximum directivity of 16.8dBi at 13.7GHz with a 3dB bandwidth of 5.6%. It can be extracted from the figure that the proposed three AIS-PRS layer antenna outperforms the single layer antenna in terms of bandwidth while keeping the same total profile (λ/2). Moreover, the directivity response of the proposed structure shows a faster roll-off. From Table II, it can be seen that the 2dB radiation bandwidth is more than doubled in the case of the proposed antenna compared with the single layer PRS antenna. Finally, the radiation patterns at the two edges of the operational bandwidth of the single layer antenna are shown in Fig. 15 for both antennas. As can be seen from the figure, a significantly improved sidelobe level is obtained with the proposed antenna, especially for the E-plane patterns. More specifically, the sidelobe level for the E-plane at 13.3GHz is -8dB and -13dB for the conventional antenna and the proposed antenna respectively. At 14.1GHz where higher order modes tend to deteriorate the radiation patterns of such type leaky wave antennas, the obtained improvement is more evident, with sidelobe levels of -3dB and -12dB for the single layer antenna and the three AIS-PRS layer antenna respectively.

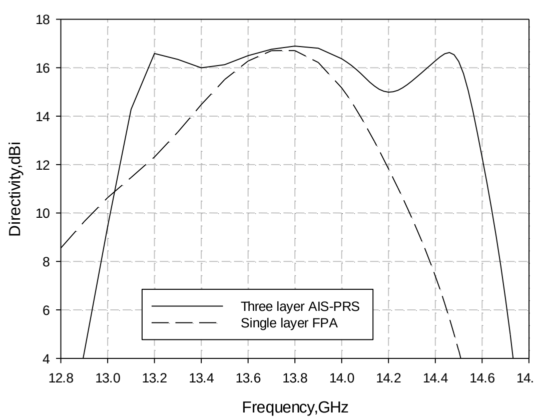

Fig. 14. Directivity vs frequency comparison between the proposed three layer AIS-PRS antenna and the single layer Fabry-Perot antenna.

TABLE II. ANTENNA PERFORMANCE COMPARISON BETWEEN THE SINGLE LAYER FABRY-PEROT ANTENNA AND THE PROPOSED THREE LAYER AIS-PRS ANTENNA

Antenna Profile	***Directivity max (dBi)***	***Bandwidth (%)***	
		2dB	***3dB***
One Layer λ/2	16.8	4.5	5.6
Three Layer AIS-PRS λ/6	16.9	10.3	10.7

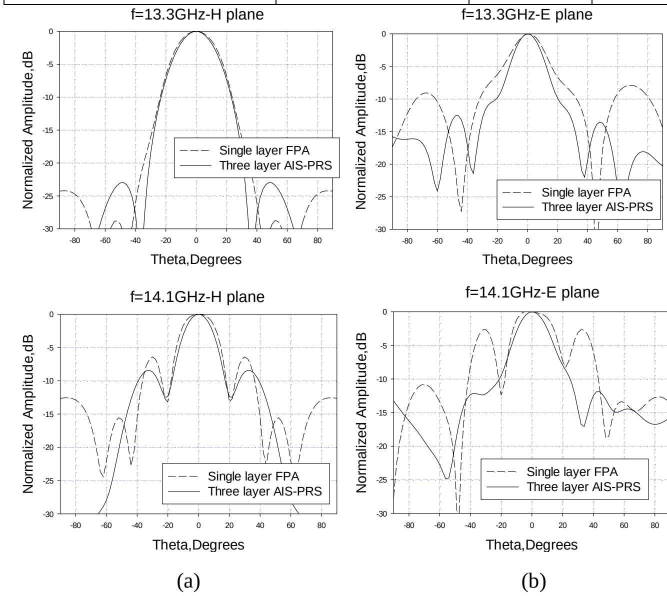

Fig. 15. Simulated H- and E-plane radiation patterns for single layer Fabry-Perot antenna and the proposed three layer AIS-PRS antenna at (a) 13.3GHz and (b) 14.1GHz.

IV. FABRICATION AND MEASUREMENTS

A prototype of the proposed antenna was fabricated and experiments were carried out to measure the antenna's performance and validate the simulation results. For each of the composite AIS-PRS surfaces, an array of 9x9 elements was etched of the copper to form the PRS side and an array of 10x10 patches was printed on the other side of a 1.55mm thick TLY-5 substrate to form the AIS (Fig. 16b). The same substrate was used for the ground plane comprising the two microstirp line fed slots (Fig. 16c). A photograph of the assembled antenna is shown in Fig. 16(a). Plastic spacers have been used to define the air cavities between the AIS-PRS surfaces and the ground plane. The measured S_{11} of the fabricated prototype along with the corresponding simulation results are shown in Fig. 17. The fabricated antenna is well matched with S11 below -10dB from 13GHz to 14.5GHz which is in good agreement with the simulation result. The simulated and measured realized gain of the antenna is presented in Fig. 18. A maximum gain of 16.3dBi has been measured at 13.7GHz with a 10.9% 3dB-bandwidth. The simulated and measured H- and E-plane radiation patterns are shown in Fig. 19 for four frequencies across the operational bandwidth of the antenna. The small discrepancies between the simulation and measurement results are attributed to fabrication tolerances of both the cavity thicknesses and the feeding slots dimensions.

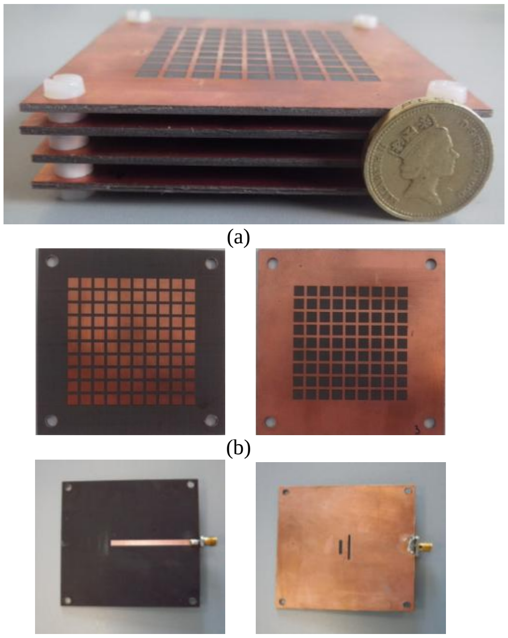

Fig. 16. (a) Photograph of the fabricated three layer AIS-PRS, (b) Both sides of AIS-PRS and (c) Both sides of the feeding structure.

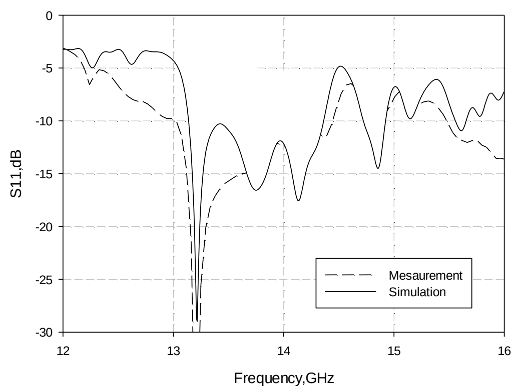

Fig. 17. Simulated and measured S11 of the proposed antenna.

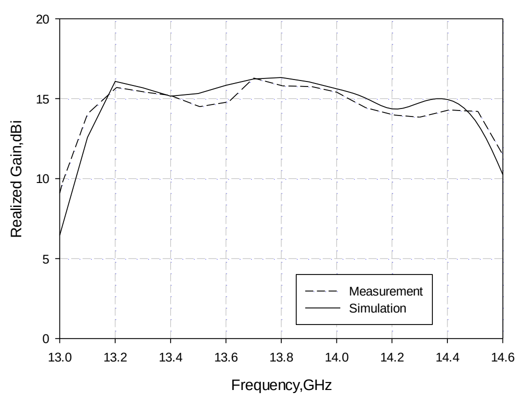

Fig. 18. Simulated and measured realized gain of the final antenna.

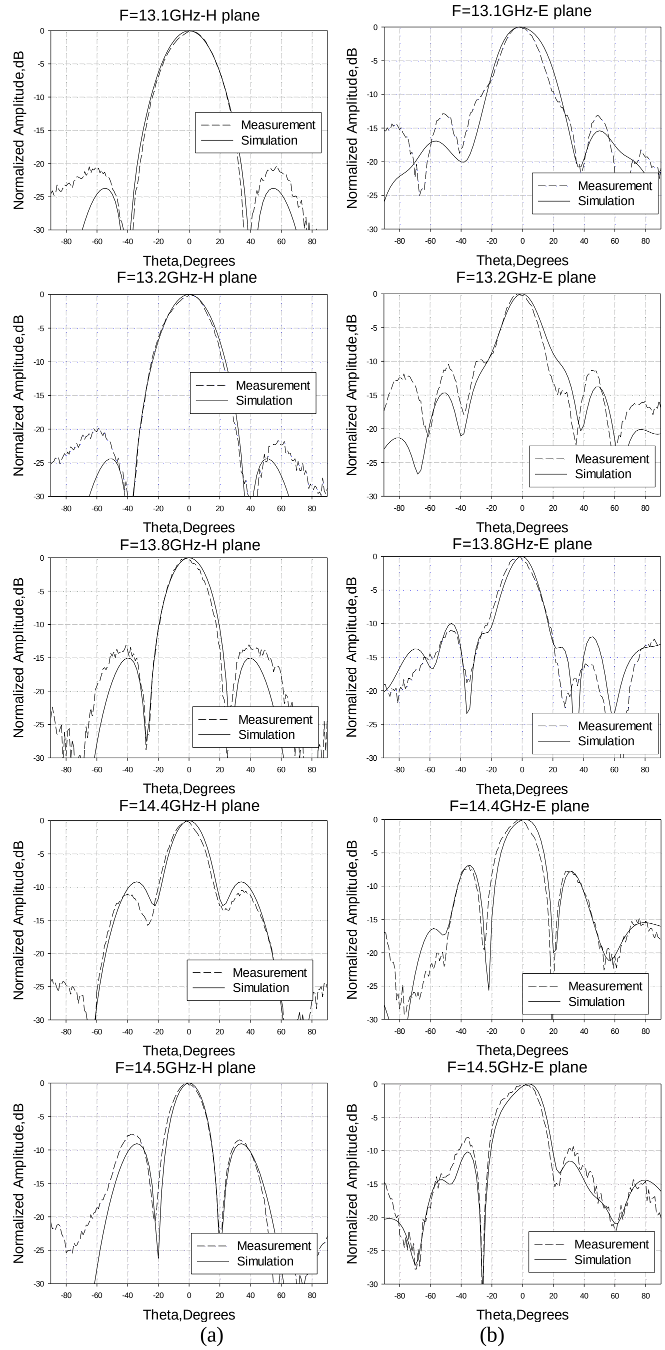

Fig. 19. . Simulated and measured radiation patterns for the (a) H-plane and (b) E-plane in five frequencies over the operational bandwidth of the antenna.

V. Conclusions

A technique for designing sub-wavelength profile antennas achieving broadband highly directive performance has been demonstrated through simulated and experimental results. Three sub-wavelength antennas have been investigated based on optimised composite double-layer arrays. A dual-resonant feeding mechanism was employed to cover the broad bandwidth of the antenna. The design of the antenna structures has been optimised using a combination of ray optics analysis and periodic full-wave simulations. Finally, a prototype of the three AIS-PRS layer antenna was fabricated and tested achieving 16.3dBi gain and 10.9% 3dB bandwidth with S_{11}

below -10dB. The antenna has a profile of λ/2 and outperforms other reported antennas with the same profile.

REFERENCES

[1] B. Temelkuaran, M. Bayindir, E. Ozbay, R. Biswas, M. M. Sigalas, G. Tuttle, and K. M. Ho, "Photonic crystal-based resonant antenna with a very high directivity," *J. Appl. Phys*., 87, 603–605, 2000.

[2] S. Enoch, G. Tayeb, P. Sabouroux, N. Guerin, and P. Vincent, "A metamaterial for directive emission," *Phys. Rev. Lett*., vol. 89, no. 21, pp. 213902-1-213902-4, Nov. 2002.

[3] E. Saenz, K. Guven, E. Ozbay, I. Ederra, R. Gonzalo, "Enhanced directed emission from metamaterial based radiation source," *Appl. Phys. Lett.*, Vol. 92, 204103-1-204103-3, 2008.

[4] Y. J. Lee, J. Yeo, R. Mittra, and W. S. Park, "Design of a high-directivity electromagnetic bandgap (EBG) resonator antenna using a frequency selective surface (FSS) superstrate," *Microwave and Optical Technology Letters*, vol. 43, no. 6, pp. 462-467, Dec. 2004.

[5] R. Gardelli, M. Albani, F. Capolino, "Array thinning by using antennas in a Fabry-Perot cavity for gain enhancement," *IEEE Trans. Antennas and Propag.*, vol.54, no.7, pp. 1979-1990, July 2006.

[6] A. Oliner. "Leaky-wave antennas," in Antenna Engineering Handbook, Third Edition, edited by *R. C. Johnson, McGraw Hill*, 1993.

[7] T. Zhao, D. R. Jackson, J. T. Williams, Hung-Yu D. Yang, and A. A. Oliner, "2-D Periodic Leaky-Wave Antennas-Part I: Metal Patch Design", *IEEE Trans. Antennas and Propag.*, vol. 53, no. 11, pp.3505-3514, Nov. 2005.

[8] T. Zhao, D. R. Jackson, J. T. Williams, Hung-Yu D. Yang, and A. A. Oliner, "2-D Periodic Leaky-Wave Antennas-Part II: Slot Design", *IEEE Trans. Antennas and Propag.*, vol. 53, no. 11, pp. 3515-3524, Nov. 2005.

[9] G.V. Trentini, "Partially reflecting sheet array", *IRE Trans. Antennas Propag.*, vol. AP-4, pp. 666-671, 1956.

[10] A. P. Feresidis, and J. C. Vardaxoglou, "High-gain planar antenna using optimized partially reflective surfaces," *IEE Proc. Microw. Antennas Propag.*, vol. 148, no. 6, Feb. 2001.

[11] A. P. Feresidis, J. C. Vardaxoglou, "A broadband high-gain resonant cavity antenna with single feed", *Proc. EuCAP* 2006, Nice, France, 2006.

[12] L. Moustafa and B. Jecko, "EBG structure with wide defect band for broadband cavity antenna applications," *IEEE Antenna Wireless Propagat. Lett.*, vol.7, pp.693-696, Nov.2008.

[13] A.R.Weily, K.P. Esselle, T.S. Bird and B.C. Sanders, "Dual resonator 1-D EBG antenna with slot array feed for improved radiation bandwidth," IET Microwaves, Antennas Propagat., vol. 1, no. 1, pp. 198-203, February 2007.

[14] Ge Yuehe, K.P. Esselle, and T.S. Bird, "The Use of Simple Thin Partially Reflective Surfaces With Positive Reflection Phase Gradients to Design Wideband, Low-Profile EBG Resonator Antennas ", *IEEE Trans. Antennas Propag.*, vol. 60, no. 2, pp. 743-750, Feb. 2012.

[15] C. Mateo-Segura, A. P. Feresidis, G. Goussetis, "Bandwidth Enhancement of 2-D Leaky-Wave Antennas With Double-Layer Periodic Surfaces," *IEEE Trans. Antennas Propag.*, vol.62, no.2, pp.586,593, Feb. 2014.

[16] K. Konstantinidis, A. P. Feresidis, P. S. Hall, "Multilayer Partially Reflective Surfaces for Broadband Fabry-Perot Cavity Antennas," *IEEE Trans. Antennas Propag*., vol.62, no.7, pp. 3474-3481, July 2014.

[17] D. Sievenpiper, Z. Lijun, R. F. Broas, N. G. Alexopoulos, and E. Yablonovitch, "High-impedance electromagnetic surfaces with a forbidden frequency band," *IEEE Trans. Microw. Theory Tech*., vol. 47, no. 11, pp. 2059–2074, Nov. 1999.

[18] S. Wang, A.P. Feresidis, G. Goussetis, J.C. Vardaxoglou, "Low-profile resonant cavity antenna with artificial magnetic conductor ground plane," *Electron. Lett*., vol.40, no.7, pp.405,406, 1 April 2004.

[19] A. P. Feresidis, G. Goussetis, S. Wang, and J. C. Vardaxoglou, "Artificial Magnetic Conductor Surfaces and Their Application to Low-Profile High- Gain Planar Antennas," *IEEE Trans. Antennas Propag.*, vol. 53, no. 1, pp. 209-215, Jan. 2005.

[20] S. Wang, A.P. Feresidis, G. Goussetis, J.C. Vardaxoglou, "High-Gain Subwavelength Resonant Cavity Antennas Based on Metamaterial Ground Planes," *IEE Proc. Antennas and Propagation*, Vol. 153, no. 1, pp.1-6, February 2006.

[21] J. R. Kelly, T. Kokkinos, and A. P. Feresidis, "Analysis and Design of Sub-wavelength Resonant Cavity Type 2-D Leaky-Wave Antennas," *IEEE Trans. Antennas and Propagation*, vol. 56, no. 9, pp. 2817-2825, Sept. 2008.

[22] C. Mateo-Segura, G. Goussetis, A. P. Feresidis, "Sub-Wavelength Profile 2-D Leaky-Wave Antennas With Two Periodic Layers," *IEEE Trans. Antennas Propag.*, vol.59, no.2, pp.416-424, Feb. 2011.

[23] L. Zhou, H. Li, Y. Qin, Z. Wei, and C. T. Chan, "Directive emissions from subwavelength metamaterial-based cavities," *Appl. Phys. Lett.*, Vol. 86, No. 10, 101101-1-101101-3, 2005.

[24] A. Ourir, A. de Lustrac, and J.-M. Lourtioz, "All-metamaterial-based sub-wavelength cavities (λ/60) for ultrathin directive antennas," *Applied Physics Lett.*, vol. 88, no. 8, pp. 84103-1–3, Feb. 2006.

[25] K. Konstantinidis, A.P. Feresidis, P. S. Hall, "Dual Subwavelength Fabry–Perot Cavities for Broadband Highly Directive Antennas," *IEEE Antenna Wireless Propagat. Lett.*, , vol.13, no., pp. 1184-1186, 2014.